Renewable Energy 75 (2015) 550–559

Contents lists available at ScienceDirect

Renewable Energy

journal homepage: www.elsevier.com/locate/renene

Energy management strategy based on receding horizon for a power hybrid system

Diego Feroldi[*, 1], Pablo Rullo, David Zumoffen [2]

French-Argentine International Center for Information and Systems Sciences (CIFASIS-CONICET-UNR-AMU), 27 de Febrero 210 bis, S2000EZP Rosario, Argentina

ARTICLE INFO

Article history:
Received 16 July 2014
Accepted 30 September 2014
Available online 1 November 2014

Keywords:
Renewable energy sources
Bioethanol
Wind energy
Solar energy
PEM fuel cells
Autoregressive models

ABSTRACT

This paper presents an energy management strategy to operate a hybrid power system with renewable sources (wind and solar), batteries, and polymeric electrolyte membrane fuel cells. The fuel cells are fed with hydrogen from bioethanol reforming. The energy management strategy uses the concept of receding horizon with predictions of the future generation from the renewable sources, the future load, and the state of charge in the battery bank. Several tests are done in order to analyze the performance of the proposed methodology. The results, compared with the case without predictions, show a reduction in the loss of power supply probability (LPSP) up to 88%.

1. Introduction

The renewable energy sources have a large amount of advantages, including sustainability, low emissions, and economical benefits. However, most of these energy sources have an intermittent behavior due to atmospheric conditions. Therefore, it is necessary to combine more than one type of renewable source to improve the robustness of the power system. This is, therefore, a hybrid power system based on renewable energy sources. One of the possible options is to combine wind and solar energy, together with a battery bank to store energy, as is presented in the paper of [7]. In this work, it is also shown the benefit of using polymeric electrolyte membrane (PEM) fuel cells to improve the robustness of the power system. The hydrogen that feeds the fuel cells is produced through bioethanol reforming.

The PEM fuel cells reinforces the power generation from the renewable sources, providing energy when is necessary according to an adequate management strategy. The proposed configuration decreases the probability of incapacity of power supply, decreasing at the same time the amount of wind turbines, solar panels, and batteries.

There are several approaches in the literature to address the energy management in hybrid power systems. These approaches are mainly based on heuristic rules that modify the system operation on the basis of the powers and state of charge in the energy storing devices [20]. In Ref. [21] a decision algorithm with a few rules is done. In Ref. [14] a more complex algorithm of decision based on rules is done. In Ref. [29] a supervisory control is done, switching the operation mode according to heuristic rules. In Ref. [18] an optimum load management strategy (minimizing a function with constraints over a period of predictions) for a wind/diesel/battery hybrid power systems is presented. In Ref. [26] a hierarchical control composed by a master control strategy and a slave control strategy is presented for an off-grid photovoltaic (PV)/wind turbine/hydrogen/battery hybrid system. In Ref. [25] a control algorithm based on DC bus voltage regulation for a fuel cell (FC)/PV/ultracapacitor system is presented. In Ref. [27] an energy management strategy based on Model Predictive Control (MPC) is presented for the same system. In Ref. [34] it is proposed a control scheme with double hysteresis. In Ref. [11] three strategies are proposed based on switching between different modes of operation, taking into account the state of charge in the batteries. In Ref. [4] three strategies based on rules are presented, taking into account also the pressure in the hydrogen tank, which is fed from an electrolyzer. In Ref. [6] a fuzzy logic based strategy is presented. In Ref. [7] an energy management strategy is proposed, which

* Corresponding author. Tel.: +54 341 4237248 304; fax: +54 341 482 1772.
E-mail address: feroldi@cifasis-conicet.gov.ar (D. Feroldi).
[1] Also with Universidad Nacional de Rosario – FCEIA-DCC, Pellegrini 250, S2000BTP Rosario, Argentina.
[2] Also with Universidad Tecnológica Nacional – FRRo, Zeballos 1341, S2000BQA Rosario, Argentina.

http://dx.doi.org/10.1016/j.renene.2014.09.056
0960-1481/

operates between five modes of operation. The strategy is formalized through the concept of finite state machine, defining modes of operation (states) and events that produces the change of state depending on the previous state and the active events according to a mapping function.

The receding horizon concept is commonly used in model predictive control formulation. In order to improve the system performance and efficiency, a prediction of meteorological variables and load power requirements must be used. In Ref. [22] a supervisory predictive control is presented, but is considered the case where the future load for certain length of time is known and environment conditions remain constant. In Ref. [32] the predicted wind, solar and temperature data are obtained and updated hourly from an official database. In Ref. [13] an autoregressive model is proposed for the prediction of wind speed and then used to calculate future wind turbines output power.

This work presents an energy management strategy based on receding horizon with a performance significantly better than the presented in Ref. [7]. This strategy takes advantage of prediction of the future generation in the power sources, the load requirement, and the evolution of the state of charge in the batteries. The predictions of the power sources and the load are performed using autoregressive models and historic data of wind speed, ambient temperature, solar radiation, and load demand. Thus, at a given time step, the energy management strategy takes decisions based on the future predictions over a finite prediction horizon. At the next time step new decisions are taken starting from the new state and over a shifted horizon, leading to a receding horizon policy. The design of the power system in this paper is done according to the results in Ref. [8].

The organization of the paper is the following. In Section 2 the description of the hybrid power system is done (electric topology and main characteristics of the system elements). In Section 3 the proposed energy management strategy is presented. In Section 4 the results are presented and confronted to the strategy without predictions. Finally, in Section 5 some conclusions and guidelines about future works are presented.

2. Description of the system

The hybrid power system is composed of several types of power sources and energy storing devices that are able to supply the load. The power sources are wind turbines, photovoltaic (PV) modules, and PEM fuel cells, while the energy storing devices are batteries. All these elements are connected to a direct-current bus through power converters. The power system has no connection to other electric grid. The PEM fuel cells are fed with high purity hydrogen from a bioethanol reforming process. Fig. 1 shows a scheme of the hybrid power system.

The detail description of the component of the power system is done in Refs. [7,8]. In particular, in the second work a methodology for the optimal sizing of the system integrated with the energy management strategy was proposed. The main objectives in the sizing process are the following: (a) achieve a reliable power supply under varying atmospheric conditions, (b) minimize the cost of the power system, and (c) minimize the bioethanol consumption. The following optimization problem is solved in the sizing methodology:

$$\min_{\mathbf{x}}\{C_T(\mathbf{x}) + \rho C_{Et}(\mathbf{x}, SOC_i, EMS)\}, \tag{1}$$

where $\mathbf{x} = [N_w, N_{PV}, N_b, N_{FC}]$ is the vector of decision variables, being N_w the number of wind turbines, N_{PV} the number of PV modules, N_b the number of batteries, and N_{FC} the number of PEM fuel cells modules. On the other hand, SOC_i is the initial state of charge ($SOC_i = SOC(t = 0)$) in the battery bank. The SOC, at discrete time $k = t/T_s$ with $k = 0,\ 1, \ldots$, is defined as follows:

$$SOC(k) = \frac{C_b^{max} - C_b^u(k)}{C_b^{max}} \times 100[\%], \tag{2}$$

where C_b^{max} is the maximum capacity of the batteries, in units of Ah, and $C_b^u(k)$ is the amount of Ah already used at time k, which can be computed as

$$C_b^u(k) = C_b^i + \sum_{j=1}^{k} \eta_c I_b(j) T_s[\text{Ah}], \tag{3}$$

where η_c is the charge/discharge battery coulombic efficiency, in this case $\eta_c = 0.975$, and I_b is the battery current in units of A ($I_b > 0$ when the battery is in discharging mode and $I_b < 0$ when it is in charging mode), T_s is the sampling time, and C_b^i is $C_b^u(k = 0)$, which corresponds to SOC_i.

The minimization is done subject to the following constraints:

$$\underline{\mathbf{x}} \leq \mathbf{x} \leq \overline{\mathbf{x}}, \tag{4}$$

which means that each decision variable in $\mathbf{x}$ is limited between a lower and an upper bound, and

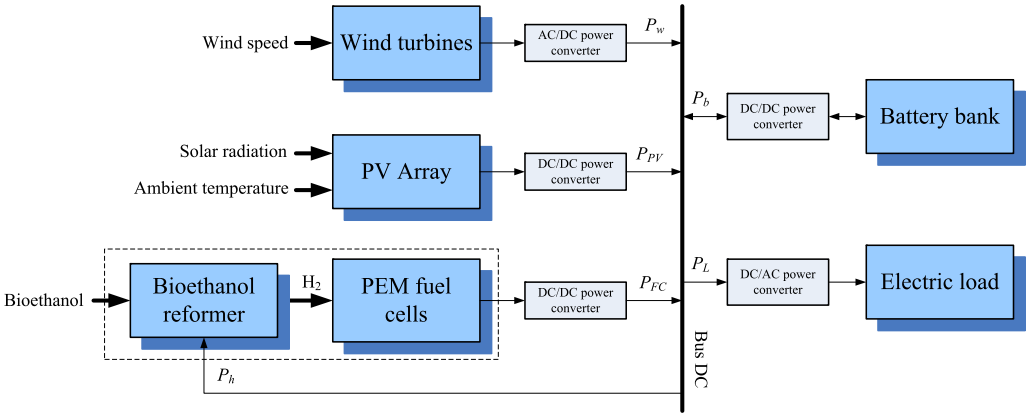

Fig. 1. Schematic diagram of the hybrid power system based on renewable sources and bioethanol.

$$\mathrm{LPSP}(\mathbf{x}) \leq \overline{\mathrm{LPSP}}, \tag{5}$$

where

$$\mathrm{LPSP}(\mathbf{x}) = \frac{T_{\mathrm{ft}}}{T_t} \times 100 \quad [\%], \tag{6}$$

is the loss of power supply probability [33], being T_t the total time in the historic data set used in the analysis (one year in this study), T_{ft} the time during which the power balance is not satisfied (for the design corresponding to the vector $\mathbf{x}$), and $\overline{\mathrm{LPSP}}$ the upper limit allowed for LPSP($\mathbf{x}$).

As a result of applying the design methodology, a set of feasible solutions is found depending on the design parameter ρ, which allows the penalization of the bioethanol consumption. In this work, the focus is on the solutions that promote the greater use of renewable energies instead of fuel cells, which decreases the bioethanol consumption. This can be seen in Fig. 2, where a bar graph shows the contribution of each power source to the load power supply. In fact, it can be seen that for $\rho \geq 50$ the contribution of the renewable power sources is greater than the contribution of the fuel cells. Therefore, the subset of designs considered in this work corresponds to the design with $\rho \geq 50$, as it is presented in Table 1.

2.1. Wind power system

The power injected by the wind power system to the DC bus between a lower limit wind speed and the rated speed can be calculated based on the steady-state power characteristics of the turbine [31]:

$$P_w(t) = \frac{1}{2} C_p(\lambda, \beta) \rho_a A v^3(t). \tag{7}$$

where A is the swept blade area, ρ_a is the air density, v is the wind velocity and C_P is the power coefficient, which expresses the efficiency of the turbine with respect to the wind power available. The power coefficient is a function of λ and the blade pitch angle β, where λ is defined as $\lambda = r\omega_m/v$, where r is the radius of the blades and ω_m is the speed angle of the turbine shaft, and can be expressed by Ref. [16]:

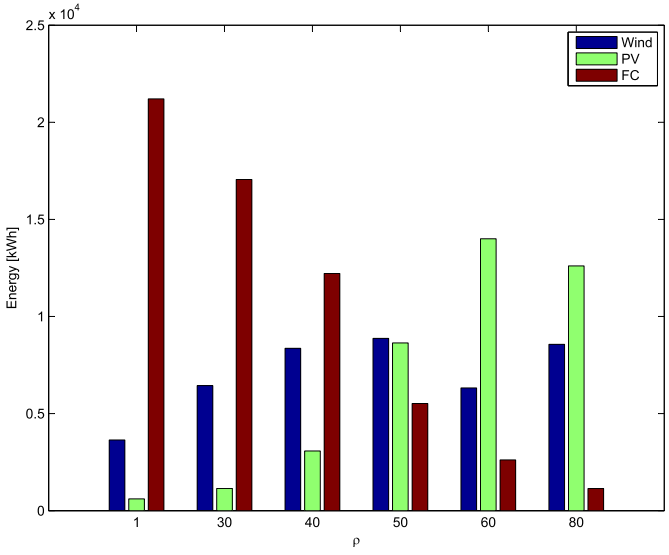

Fig. 2. Bar graph showing the energy supply of each power source with the different designs.

Table 1
Set of optimal designs as a function of parameter ρ.

ρ	N_w	N_{PV}	N_b	N_{FC}
50	3	18	5	3
60	2	29	7	2
80	3	30	9	1

$$C_p(\lambda, \beta) = \frac{1}{2}\left(\frac{rC_f}{\lambda} - 0.022\beta - 2\right) e^{-0.255\frac{rC_f}{\lambda}}, \tag{8}$$

where C_f is a design constant of the blades. The values of the parameters used are as follows: $\rho_a = 1.2$ kg m^3, $r = 1.6$ m, $A = 8$ m^2, $C_f = 19.92$. Thus, the wind turbines have a nominal power of 2 kW at rated wind speed of 9 m s^{-1}. The pitch angle of the blades and the speed angle can be adjusted, allowing to maximize the power extracted from the wind turbines according to the actual wind speed [1]. When the load is below the rated power P_w^r, the turbine operates at variable rotor speeds, fixing the blade pitch angle. For wind speeds above the rate value, the turbine is operated at constant output power, varying the blade pitch angle [2]. On the other hand, the wind turbine is stopped for wind speeds below a lower limit ($v_l = 1.5$ m s^{-1}) and above an upper limit ($v_u = 20$ m s^{-1}). Note that even though this model is quite simple, it is suitable to be used into the methodology of sizing and energy management. A more complex model can be impractical since the mentioned methodology involves a mixed integer optimization [8].

2.2. Solar power system

A PV cell presents a voltage–current and power-current nonlinear characteristic which depend mainly of insolation and temperature. The equivalent circuit of the model consists of current source, a diode and a serial resistance. The output current of the cell (I_{pv}) can be expressed by Ref. [30]:

$$I_{\mathrm{pv}}(t) = I_{\mathrm{ph}}(t) - I_{\mathrm{rs}}(t)\left(\exp\left(\frac{q\left(V_{\mathrm{pv}}(t) + I_{\mathrm{pv}}(t)R_s\right)}{A_c \mathrm{KT}(t)}\right) - 1\right), \tag{9}$$

where I_{ph} is the generated current under a given insolation, I_{rs} is the cell reverse saturation current, V_{pv} is the voltage level on the PV cell terminals, q is the charge of an electron, R_s is the intrinsic cell resistance, A_c is the cell deviation from the ideal p–n junction characteristic, K is the Boltzman constant, and T is the cell temperature. The photocurrent current depends on insolation and temperature according to the following expression:

$$I_{\mathrm{ph}}(t) = \left(I_{\mathrm{sc}} + K_l(T(t) - T_r)\right)\lambda(t) \Big/ 100, \tag{10}$$

where I_{sc} is the short-circuit cell current at the reference temperature and isolation, K_l is the short-circuit current temperature coefficient and λ is the insolation in mW cm^{-2}.

The reverse saturation current depends on temperature according to the following expression:

$$I_{\mathrm{rs}}(t) = I_{\mathrm{or}}\left(\frac{T(t)}{T_{\mathrm{ref}}}\right)^3 \exp\left(\frac{qE_{\mathrm{go}}(1/T_r - 1/T(t))}{KA_c}\right), \tag{11}$$

where I_{or} is the reverse saturation current at the reference temperature T_{ref} and E_{go} is the band-gap energy of the semiconductor used in the cell (values in Table 2).

PV cells are connected in serial-parallel configurations forming modules, which are the typical commercial unit. In order to reach

Table 2
Parameters of the solar system.

q	1.6×10^{-19} C
A_c	1.6
K	1.3805×10^{-23} Nm K^{-1}
K_I	0.0017 A °C^{-1}
I_{or}	2.0793×10^{-6} A
T_{ref}	301.18 K
E_{go}	1.10 V
I_{sc}	3.27 A

appropriate voltage and power levels, modules can be arranged with a similar architecture on arrays [28]. The solar power system is composed of a PV array connected to the DC bus through a DC/DC power converter. Thus, the available current for a PV module can be expressed as follows:

$$I_{PV}^{av}(t) = n_p I_{ph}(t) - n_p I_{rs}(t)\left(\exp\left(\frac{q\left(V_{PV}(t) + I_{pv}(t)R_s\right)}{n_s A_c K T(t)}\right) - 1\right), \tag{12}$$

where V_{PV} is the voltage level in the PV module terminals, n_p is the number of parallel strings and n_s is the number of serial connected cells per string. Therefore, the available power generation from a PV module is

$$P_{PV}^{av}(t) = V_{PV}(t) I_{PV}^{av}(t). \tag{13}$$

The solar modules have nominal power of 150 W at global radiation of 1 kW m^{-2} and temperature of 25 °C. The number of modules is determined through the sizing methodology in Ref. [8].

In a PV module, the generated power depends on the solar radiation, the temperature, and the module voltage. Therefore, there is a point for each solar radiation and temperature where the maximum power is obtained. This point can be experimentally obtained, that is to determine the necessary module voltage according to the actual solar radiation and temperature. However, this methodology is dependent of each particular module. Besides, it is necessary to measure the radiation and the temperature. To overcome these drawbacks, there are algorithms capable of dealing with the maximum power point tracking (MPPT). In particular, a maximum power point tracking (MPPT) scheme is presented in Ref. [17], where the maximum power operating point is tracked accurately based on extremum-seeking control.

2.3. Reformer-fuel cell power system

The bioethanol processor system (BPS) is composed of a main reactor, the ethanol steam reformer (ESR) which is in charge of the conversion of bioethanol to hydrogen. The output stream in this step has inappropriate concentration levels of carbon monoxide and the PEM Fuel Cell catalyst could be damaged. Therefore, a cleaning stage must be included. Three reactors integrate this stage, two Water Gas Shift, one of high temperature (HTS) and the other of low temperature (LTS) and a preferential oxidation of carbon monoxide (CO-PrOx) reactor, where oxidation of CO into CO_2 is made. In Ref. [23] a model predictive control strategy is applied to meet the hydrogen quality requirements of the PEM fuel cell.

The main reaction in the ESR is endothermic, thus it requires a heat supply. The amount of heat necessary to supply is $\Delta H_{298}^{o} = 254.8$ kJ mol^{-1}. In this work this heat is provided through a heating resistor (P_h), which is supplied with energy from DC bus. From the stoichiometric equation of the reaction can be obtained de required power of the heater:

$$P_h = \frac{W_{H_2} \Delta H_{298}^{0}}{4} \tag{14}$$

where W_{H_2} is the rate of hydrogen consumed by the PEM fuel cell.

PEM fuel cells are electrochemical devices that convert the chemical energy stored in hydrogen directly into electricity with high efficiency. The cell anode is fed with hydrogen and a cathode fed by air. The rate of hydrogen consumed in the fuel cell anode is a function of the fuel cell current:

$$W_{H2,\,rct} = \frac{M_{H_2} n}{2F} I_{FC}, \tag{15}$$

where $W_{H_2,\,rct}$ is the rate of hydrogen reacted, $M_{H_2} = 2.016 \times 10^{-3}$ kg mol^{-1} is the molar mass of oxygen, n is the number of cells in the stack, $F = 96,485$ C mol^{-1} is the Faraday number, and I_{FC} is the stack current. This is the amount of hydrogen that is required to the bioethanol processor system.

The power modules based on PEM fuel cells need auxiliary services (pumps, compressor, control system, etc) for its operation, which are fed from fuel cell terminals [15]). This fact define a power lower limit, below which is not suitable to operate because the parasitic load is too large, reducing the efficiency. The power upper limit is defined by the rated power of the stack:

$$\underline{P_{FC}} \le P_{FC}(t) \le \overline{P_{FC}}. \tag{16}$$

On the other hand, the fuel cell power cannot be increased faster than a certain power rise rate ($\overline{\Delta P_{FC}}$) to avoid a lack of reactants and the power cannot be decreased faster than a certain power fall rate ($\underline{\Delta P_{FC}}$) to prevent overpressure into the stack:

$$\underline{\Delta P_{FC}} \le \Delta P_{FC}(t) \le \overline{\Delta P_{FC}}, \tag{17}$$

where $\Delta P_{FC}(t) = P_{FC}(t) - P_{FC}(t - \Delta T)$ and ΔT is the sample time. The PEM fuel cell modules have a nominal power of 1, 2 kW.

On the other hand, the fuel cell power cannot be increased faster than a certain power rise rate ($\overline{\Delta P_{FC}}$) to avoid a lack of reactants and the power cannot be decreased faster than a certain power fall rate ($\underline{\Delta P_{FC}}$) to prevent overpressure into the stack:

2.4. Energy storage system

The variability of the renewable sources and the fact of being an stand-alone application implies the need to use an energy storage system (ESS) [9]. In this paper, we have chosen to use a bank of lead-acid batteries because they are the least expensive for hybrid energy system applications. The main characteristics of the battery bank are given in Table 3.

The battery model used consists of a voltage source, which represents the open circuit voltage (V_{oc}) and a serial resistance (R_{int}). Thus, the terminal voltage of the battery can be expressed by $V_{bat} = V_{oc} - I_{bat} R_{int}$. Both V_{oc} and R_{int} depend on the battery state of charge (SOC). These relationships are implemented by data vectors indexed by SOC, based on experimental data of the

Table 3
Parameters of the batteries.

Parameter	Value
Type battery	Lead-acid
Nominal capacity of each battery	104 Ah
Nominal voltage	13 V
Minimum voltage	9.5 V
Maximum voltage	16.5 V

manufacturers that can be obtained from the modeling tool of hybrid automation systems called ADVISOR [12].

The SOC must be kept within certain limits to ensure good performance and battery life. In this work the lower and upper limits are $\underline{SOC} = 20\%$ and $\overline{SOC} = 100\%$, respectively. Besides, the SOC, defined in 2, depends on the charge/discharge battery coulombic efficiency η_c, in this case $\eta_c = 0.975$.

On the other hand, the battery current should also be limited. The lower and upper limits ($\underline{I_b}$ and $\overline{I_b}$) depend on V_{oc} and R_{int} through the following expressions:

$$\begin{aligned} \underline{I_b} &= \frac{\left(V_{oc} - \overline{V_b}\right)}{R_{int}} \quad \text{during charging} \\ \overline{I_b} &= \frac{\left(V_{oc} - \underline{V_b}\right)}{R_{int}} \quad \text{during discharging} \end{aligned}, \tag{18}$$

where $\underline{V_b}$ and $\overline{V_b}$ are the lower and upper limits in the battery bank voltage, respectively.

3. Energy management strategy

The energy management strategy is in charge of commanding the operation of the system with the objective of ensuring the power balance with constraints between the power sources, the batteries, and the load. The power balance in the direct-current bus can be expressed as follows:

$$P_L = P_w + P_{PV} + P_{FC} + P_b - P_h, \tag{19}$$

where P_w, P_{PV}, P_{FC}, and P_b the powers supplied to the to the direct-current bus by the turbines, the PV array, the fuel cells, and the batteries, respectively. On the other hand, P_L is the power required by the load and P_h is the power consumed by the heater in the reformer. It is assumed that the power converters DC/DC, AC/DC, and DC/AC have constant efficiencies ($\eta_{DD} = 0.95$ and $\eta_{AD} = \eta_{DA} = 0.9$).

Due to operative limitations, the power balance in (19) is subject to the following constraints:

$$0 \le P_w \le P_w^{av}, \tag{20}$$

$$0 \le P_{PV} \le P_{PV}^{av}, \tag{21}$$

$$\underline{P_{FC}} \le P_{FC} \le \overline{P_{FC}}, \tag{22}$$

$$\underline{\Delta P_{FC}} \le \Delta P_{FC} \le \overline{\Delta P_{FC}}, \tag{23}$$

$$P_b^c \le P_b \le P_b^d, \tag{24}$$

where P_w^{av} is the power available from the wind turbines; P_{PV}^{av} is the power available from the PV array; $\underline{P_{FC}}$ y $\overline{P_{FC}}$ are the lower and upper limits in the power from the fuel cell modules, respectively; $\underline{\Delta P_{FC}}$ y $\overline{\Delta P_{FC}}$ are the lower and upper limits in the fall rate and rise rate of the power from the fuel cell modules, respectively; P_b^c y P_b^d are the maximum available powers (charge and discharge, respectively) from the battery bank, which depend on the state of charge.

The proposed energy management strategy can be described through the concept of finite state machine, where each state defines an operation mode of the power system and the change of state is based on events that involve the comparison between available powers, load required, and state of charge in the batteries.

In the energy management strategy presented in Ref. [7] the events are based on the comparative between magnitudes in the present time. In the energy management strategy here proposed the events take into account the evolution of the magnitudes over a future finite horizon. For that, a prediction over the future horizon is done using time series.

3.1. Time series

A time series is a sequence of values taken sequentially in time. Generally, these values are observations of a variable taken at discrete, equispaced intervals of time [3]. The use at discrete time k of available information from the current and previous values $k,\ k-1,\ k-2, \ldots, k-w$, makes possible to forecast the value at some future time $k+p$. Note that it is used the abbreviated notation k to refer to the time $t = k\,T_s$ with $k = 0,\ 1, \ldots$, where T_s is the sampling time.

The time series data has a particular time order and, generally, the data is not associated to measure input signals. In this sense, the modeling process has to consider this structure in the model. The time series models can be used to predict the future behavior of a variable as a function of past and present values of the time series. In the field of time series analysis this is known as forecasting, marking a clear difference with the system identification field where it is known as prediction.

3.2. Modeling and parameter estimation

A discrete-time generic polynomial model utilizes the concept of transfer function to represent the input–output ($u(k) - y(k)$) and noise–output ($e(k) - y(k)$) relations through the following expression (Ljung, 1999):

$$A(z^{-1})y(k) = \frac{B(z^{-1})}{F(z^{-1})}u(k) + \frac{C(z^{-1})}{D(z^{-1})}e(k), \tag{25}$$

where A, B, C, D, and F are polynomials in the time-shift operator z^{-1}, with orders n_a, n_b, n_c, n_d y n_f, respectively, and $e(k)$ is a white noise with variance λ.

In practice, it is common not to use all the polynomials in (25). This fact generates a wide variety of type of model: Finite Impulse Response (FIR), Autoregressive (AR), Autoregressive with exogenous input (ARX), etc.

Given that the time series in this work are scalar, it is assume that the signals are represented through the AR structure as follows:

$$\left(1 + a_1 z^{-1} + a_2 z^{-2} + \ldots + a_{n_a} z^{-n_a}\right) y(k) = e(k), \tag{26}$$

which represents, according to (25), that $u(k) = 0$, $C(z^{-1})/D(z^{-1}) = 1$ and $A(z^{-1}) = 1 + a_1 z^{-1} + a_2 z^{-2} + \ldots + a_{n_a} z^{-n_a}$.

Therefore, the proposed model in the form of linear regressors results:

$$\widehat{y}(k) = \theta^T \varphi(k) = \varphi^T(k)\theta, \tag{27}$$

where $\widehat{y}(k)$ is the prediction given by the model one step ahead (not including the noise),

$$\theta = [a_1, a_2, \ldots, a_{n_a}]^T \tag{28}$$

is the vector of parameters, and

$$\varphi(k) = [y(k-1), y(k-2), \ldots, y(k-n_a)]^T \tag{29}$$

is the regressor. Assuming that the values of the vector of parameters θ are unknown but N values of the time series $Y^N = [y(1), y(2), \ldots, y(N)]$ are collected, it is possible to use the structure of the model in (27)–(29) in such a way that the predictions $\widehat{y}(k)$ and the observations of the data set are adjusted in the least-square sense. In fact, if the following functional is stated:

$$V_N\left(\theta, Y^N\right) = \frac{1}{N}\sum_{k=1}^{N}\left(y(k) - \varphi(k)^T\theta\right)^2, \tag{30}$$

the least-square estimation can be expressed as follows:

$$\widehat{\theta}_N = \arg\min_{\theta} V_N\left(\theta, Y^N\right), \tag{31}$$

where $\widehat{\theta}_N$ represents that N input–output values are used in the calculation.

Setting $dV_N(\theta, Y^N)/d\theta = 0$, it is possible to find that the lest-square estimation results:

$$\widehat{\theta}_N^{LS} = \left[\sum_{k=1}^{N}\varphi(k)\varphi(k)^T\right]^{-1}\sum_{k=1}^{N}\varphi(k)y(k) = \left(\Phi_N\Phi_N^T\right)^{-1}\Phi^N Y^N, \tag{32}$$

with $\Phi_N = [\varphi(1), \varphi(2), \ldots, \varphi(N)]$.

3.3. Forecasting or prediction

The model proposed in (27)–(29) can be utilized to carry out forecasts (predictions) of the future values of a time series based on historic data along the horizon p. In fact, it is possible to formulate the following iterative evaluation starting from the present time k until $k+p$:

$$\begin{aligned}
\widehat{y}(k+1) &= \theta^T[y(k), y(k-1), \ldots, y(k-n_a+1)]^T,\\
\widehat{y}(k+2) &= \theta^T[\widehat{y}(k+1), y(k), \ldots, y(k-n_a+2)]^T,\\
&\vdots\\
\widehat{y}(k+p) &= \theta^T[\widehat{y}(k-1+p), \ldots, y(k-n_a+p)]^T,
\end{aligned} \tag{33}$$

where it is observed that the regressor $\varphi(k+p) = [\widehat{y}(k-1+p), \ldots, y(k-n_a+p)]^T$ progressively incorporates the predictions of the time series done in previous steps, i.e. $\widehat{y}(k-1+p), \ldots, \widehat{y}(k+1)$. Note that the predictions in (27)–(29) are done with information until instant k.

However, the performance of the predictions along the horizon p can be improved if the regressor is updated progressively with new incoming (measured) data. In fact, the predictions in the horizon $k+1$ to $k+p$ are based on real measurements in the temporal window k to $k-n$, where n is the AR model order. In the next time step, the real measurements at $k+1$ are now available, which enable to repeat the overall prediction process. The mentioned procedure is shown in Fig. 3, in this case, for two particular instances. In $k = 1600$ h the prediction horizon is evaluated from $k+1 = 1601$ to $k+5 = 1605$ by using real historical measurements from k to $k-n$. In the next step $k+1 = 1601$ the prediction horizon is moved to $k+2 = 1602$ to $k+6 = 1606$, but in this case with the real measurement for $k+1$ already incorporated to the regressor. This methodology is known as receding horizon and avoids extreme divergences for predictions.

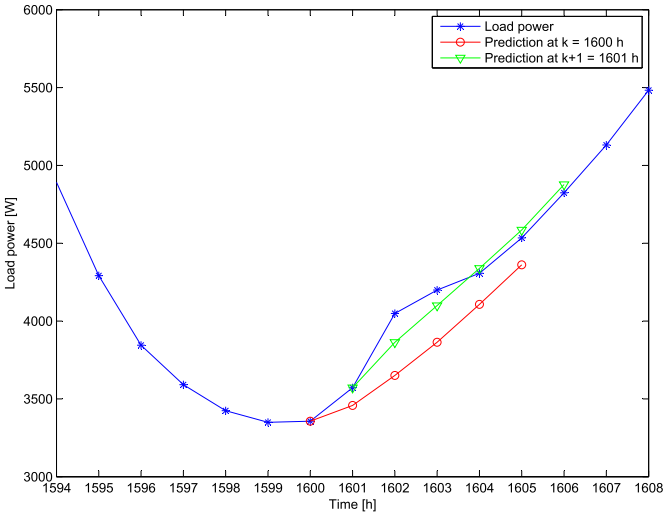

Fig. 3. Illustrative example of the prediction procedure using the receding horizon concept.

4. Energy management strategy based on receding horizon

The energy management strategy based on receding horizon can be described through the finite state machine, which consist of states and events that change the state [24]. A finite state machine can be define as a 4-tuple $\langle S, \Sigma, \delta, s0\rangle$, where:

- $S = \{s_1, s_2, \ldots, s_n\}$ is the set of n modes (or nodes) in the statechart.
- $\Sigma = \{1, 2, \ldots, m\}$ is the set of m events.
- $\delta : S \times \Sigma \rightarrow S$ is the function that maps the next states as a function of the current state and the active events in Σ (see Table 4).
- $s_0 \in S$ is the initial state.

In the proposed strategy, the main generation role is in charge of the wind turbines while the PV array have a secondary priority. The motivation for this criterion is because of the intended application is in geographical areas with wealthy wind regimes. Therefore, the first priority is that the proposed energy management strategy operates the wind turbines at its maximum power point so long as possible. Thus, the role of the solar subsystem is to reinforce the wind subsystem. Similarly, the battery bank also reinforces the wind-solar subsystems. On the other hand, the fuel cell modules have the lower priority to avoid the bioethanol consumption. Thus, taking into account this objectives and the constraints in (20)–(24),

Table 4
State/event function ($\delta : S \times \Sigma \rightarrow S$).

Current state	Event	Next state
s_1	5	s_4
	6	s_5
	1	s_2
s_2	5	s_4
	6	s_5
	2	s_1
	3	s_3
s_3	5	s_4
	6	s_5
	4	s_2
s_4	7	s_1
s_5	8	s_1

five states $S = \{s_1, s_2, \ldots, s_5\}$, with initial state $s_0 = s_1$, and eigth events $\Sigma = \{1, 2, \ldots, 8\}$, are defined. Fig. 4 shows the statechart corresponding to the proposed energy management strategy.

The description of the five states is the following:

- In mode s_1 the wind system operates at maximum power to supply the load and to recharge the batteries with the remaining energy. The solar panels and the reformer-fuel cells are turned off.
- In mode s_2 the wind system and the solar system operate at maximum power. The two power sources supply the load and the batteries operate in charging mode. The reformer-fuel cells are turned off.
- In mode s_3 the wind system and the solar system operate at maximum power. The batteries also supply the load (discharging mode) to meet the power balance. The reformer-fuel cells are turned off.
- In mode s_4 the wind system and the solar system are turned off. The batteries supply the load (discharging mode). The reformer-fuel cells are turned off.
- In mode s_5 the wind system and the solar system operate at maximum power. The reformer-fuel cells are turned on (variable load). The batteries supply or absorb the necessary power (discharging/charging mode) to meet the power balance.

The events that produce changes in the system state take into account the predictions in the future behavior of the available power in the renewable sources (wind and solar), the load, and the evolution of the state of charge in the batteries. The available powers depend, in turn, on the behavior of the atmospheric conditions (wind speed, solar radiation, and ambient temperature). With the power predictions over a horizon p, it is possible to compute the available energy during the same period using trapezoidal integration:

$$\widehat{E}_j(k) = \frac{T_s}{2}\sum_{i=1}^{p}\left(\widehat{p}_j(k+i) + \widehat{p}_j(k+i-1)\right), \tag{34}$$

where j is a sub-index according to the particular power (L for load, PV for solar, w for wind, and b for battery).

Therefore, at a given instant k, it is done the prediction over the horizon p, that is until $k+p$, of the variables according to (33). Then, the events are evaluated on the basis of the predictions and the new state in $k+1$ is computed according to the current state in k and the function $\delta : S \times \Sigma \rightarrow S$. This also can be seen in Fig. 4. In the next instant, $k+1$, the predictions are computed again starting from the current value in $k+1$ over the horizon p, that is until $k+p+1$. With this predictions, the events are evaluated again and a new state for $k+2$ is computed from the state in $k+1$. This methodology is known as receding horizon. Note that at every time the predictions are done from the measured values in the current time to avoid excessive divergences between the predictions and the real magnitudes.

The description of the events in the energy management strategy is the following:

- The event 1 occurs when energy required by the load along the prediction horizon p is greater than the available energy from the turbines in the same period: $\widehat{E}_L(k) > \widehat{E}_w^{\mathrm{av}}(k)$, where

$$\widehat{E}_L(k) = \frac{T_s}{2}\sum_{i=1}^{p}(\widehat{p}_L(k+i) + \widehat{p}_L(k+i-1)) \tag{35}$$

and

$$\widehat{E}_w^{\mathrm{av}}(k) = \frac{T_s}{2}\sum_{i=1}^{p}\left(\widehat{p}_w^{\mathrm{av}}(k+i) + \widehat{p}_w^{\mathrm{av}}(k+i-1)\right). \tag{36}$$

- On the contrary, the event 2 occurs when $\widehat{E}_L(k) < \widehat{E}_w^{\mathrm{av}}(k)$.
- The event 3 occurs when $\widehat{E}_L(k) > \widehat{E}_w^{\mathrm{av}}(k) + \widehat{E}_{\mathrm{PV}}^{\mathrm{av}}(k)$, where

$$\widehat{E}_{PV}^{av}(k) = \frac{T_s}{2}\sum_{i=1}^{p}\left(\widehat{p}_{PV}^{av}(k+i) + \widehat{p}_{PV}^{av}(k+i-1)\right). \tag{37}$$

- On the contrary, the event 4 occurs when $\widehat{E}_L(k) < \widehat{E}_w^{\mathrm{av}}(k) + \widehat{E}_{\mathrm{PV}}^{\mathrm{av}}(k)$.
- The event 5 occurs when $\widehat{\mathrm{SOC}}(k+i) \geq \overline{\mathrm{SOC}}$ for all $i = 1, \ldots, p$, where $\overline{\mathrm{SOC}} = 100\%$ is the upper limit in the allowed state of charge in the battery bank.

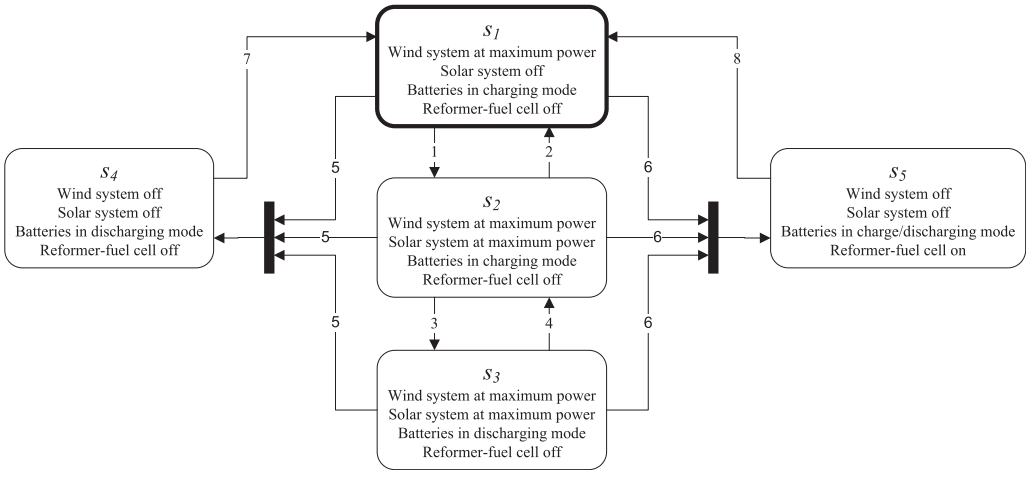

Fig. 4. Description of the energy management strategy through finite state machine.

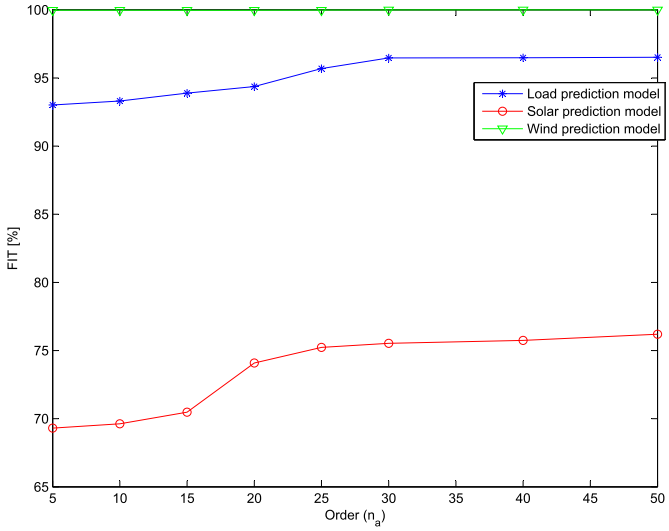

Fig. 5. Fit percentage as function of the model order.

- The event 6 occurs when $\widehat{E}_L(k) > \widehat{E}_w^{\text{av}}(k) + \widehat{E}_{\text{PV}}^{\text{av}}(k) + \widehat{E}_b^d(k)$ and $\widehat{\text{SOC}}(k+i) \leq \underline{\text{SOC}}$ for all $i = 1, \ldots, p$, where $\underline{\text{SOC}} = 20\%$ is the lower limit allowed in the state of charge in the batteries and

$$\widehat{E}_b^d(k) = \frac{T_s}{2} \sum_{i=1}^{p} \left(\widehat{p}_b^d(k+i) + \widehat{p}_b^d(k+i-1) \right), \tag{38}$$

- being $p_b^d(k)$ the available power from the batteries (discharge mode) in k.
- The event 7 occurs when $\widehat{\text{SOC}}(k+i) < (\overline{\text{SOC}} - \Delta\text{SOC}_t)$ for all $i = 1, \ldots, p$, where $\Delta\text{SOC}_t = 20\%$ is the switching threshold to avoid successive commutations around $\overline{\text{SOC}}$.
- Finally, the event 8 occurs when $\widehat{\text{SOC}}(k+i) > (\underline{\text{SOC}} + \Delta\text{SOC}_t)$ for all $i = 1, \ldots, p$.

5. Results and discussion

According to the statements in Section 3.2, three prediction models were developed corresponding to the prediction of the wind power, the solar power, and the load required. To develop these prediction models, historic data corresponding to the solar radiation (accessed from Ref. [10]), wind speed and ambient temperature (accessed from Ref. [19]), and load (accessed from Ref. [5]) is employed. Two data sets are constructed: the estimation data set and the validation data set. Each dat set corresponds to a different year, sampled every hour.

First, the wind power and the solar power are computed with the wind speed, solar radiation, and ambient temperature corresponding to the estimation data set. This is done using the fully parameterized first principles computational models of the wind subsystem ($P_w = f(v)$) and the solar subsystem ($P_{\text{PV}} = g(\lambda, T)$) developed in Ref. [7]. Then, with these powers, the prediction models for the wind subsystem and the solar subsystem are developed, according to Section 3.2. On the other hand, the load

Table 5
Order and fit percentage of the prediction models.

	Order (n_a)	FIT [%]
Load prediction model	15	93.89
Solar prediction model	20	74.09
Wind prediction model	5	99.97

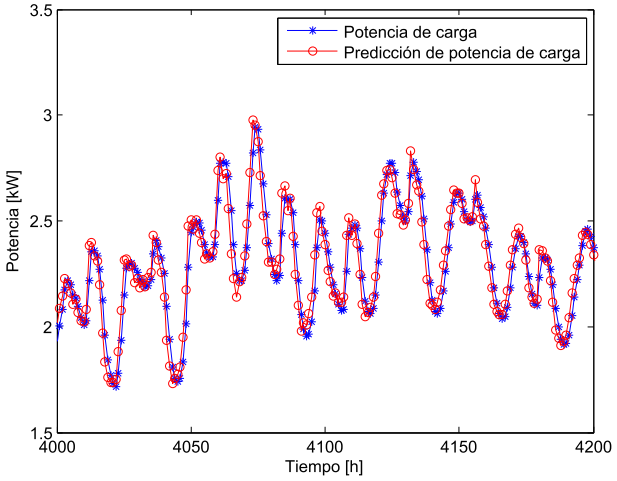

(a) Load power

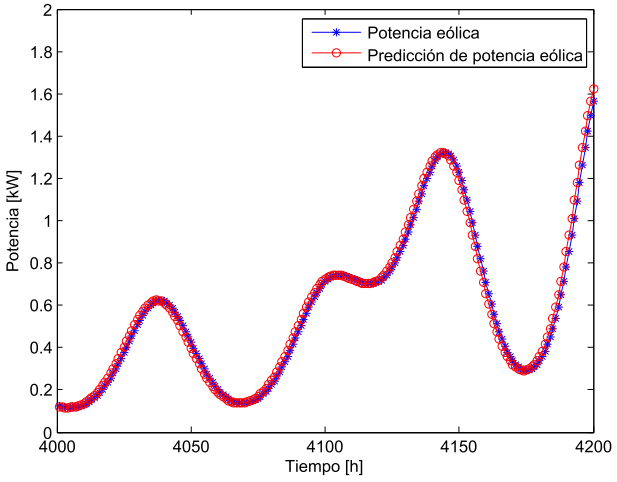

(b) Wind power

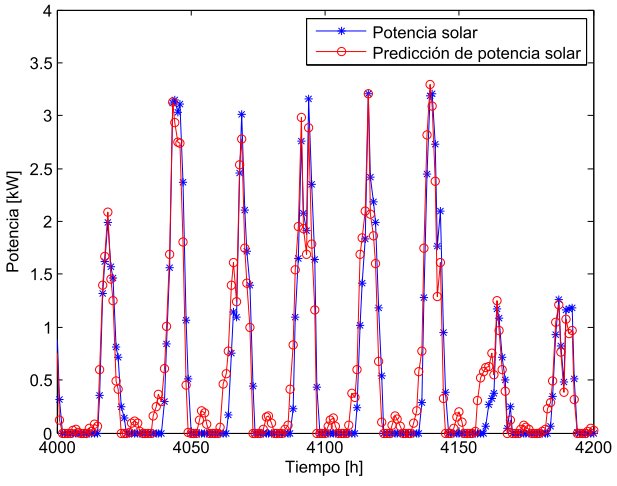

(c) Solar power

Fig. 6. Predictions using the receding horizon policy.

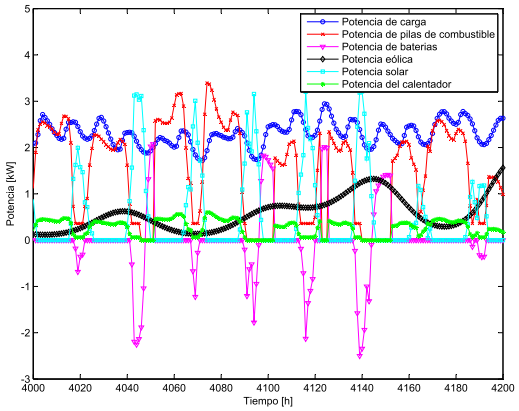

(a) Power split to meet the load requirements according to the EMS based on receding horizon.

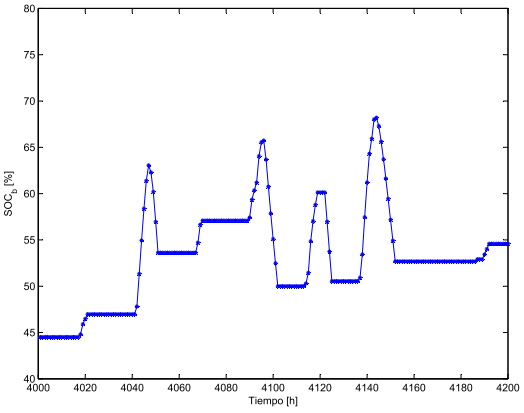

(b) State of charge in the battery bank (SOC).

Fig. 7. Simulation results (period between 4000 and 4200 h).

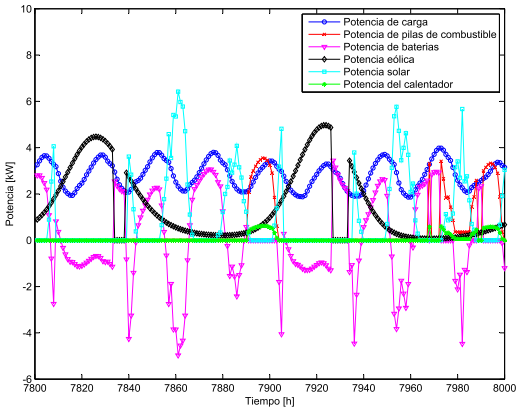

(a) Power split to meet the load requirements according to the EMS based on receding horizon.

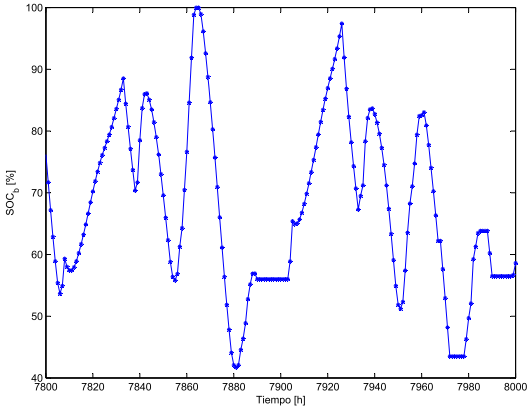

(b) State of charge in the battery bank (SOC).

Fig. 8. Simulation results (period between 7800 and 8000 h).

prediction model is developed directly from the estimation data set of the load required historic data.

The order (n_a) of the prediction models were adjusted to achieve a properly fitting using a searching method. The fit percentage as a function of the model order is shown in Fig. 5, while the orders chosen the after the fitting process are shown in Table 5. The fit percentage is calculated as follows:

$$\mathrm{FIT} = 100\left[1 - \frac{||y - \hat{y}||}{||y - \mathrm{mean}(y)||}\right], \tag{39}$$

where y is the validation data and $\hat{y}$ is the prediction done by the model.

Then, the predictions over the prediction horizon are computed using these models. The prediction horizon is set to $p = 5$ and $T_s = 1$ h. The window of historic data w that is provided to each model to perform the prediction at time k, that is $y(k)$, $y(k-1)$, $y(k-2), \ldots, y(k-w+1)$, where y is the variable to predict, is set equal to the order of the model n_a. If $w > n_a$, the remaining data $(y(k-n_a), y(k-n_a-1), \ldots, y(k-w+1))$ is not taken into account. On the contrary, if $w < n_a$ the precision in the fitting is lower because the model is not fully exploited.

In order to illustrate the performance of the models obtained, the evolution of the load power, the wind power, and the solar power are shown in Fig. 6(a), (b), and (c), respectively, together with the corresponding predictions. It is worth mentioning that these figures show only the first prediction value used at each step, according to the receding horizon approach. Besides, in this figures only a fragment of the total data set is shown, to appreciate how the predictions follows their corresponding variable.

In order to show the performance of the energy management strategy, simulation results corresponding to the design with $\rho = 50$ are presented in Fig. 7(a) and (b). Fig. 7(a) shows a portion (from 4000 h to 4200 h) of the evolution of the load power, the evolution of the powers from the sources (turbines, panels, and fuel cell), and the evolution of the power from the batteries as a result of applying the energy management strategy. On the other hand, Fig. 7(b) shows the evolution of the state of charge in the battery bank.

Analogously, in Fig. 8(a) and (b), simulation results for other period (7800–8000 h) are shown. In this period the renewable sources can supply more power and therefore the use of the fuel

Table 6
Comparison between the performance of both strategies in terms of *LPSP* for each design with different parameter ρ.

ρ	LPSP 1 [%]	LPSP 2 [%]	Improvement [%]
50	4.12	0.49	88
60	4.18	1.05	75
80	4.04	2.82	30

cells is lower with the consequent reduction in the bioethanol consumption.

In Table 6 a comparison between the performance of both strategies is presented. The parameter used to evaluate the performance is the LPSP. The design requirement for this parameter in both strategies was set to LPSP $< \overline{\text{LPSP}} = 5\%$. In fact, it can be seen that LPSP 1, corresponding to the strategy without predictions, is lower than $\overline{\text{LPSP}}$ for all the designs (varying the parameter ρ). However, with the new strategy based on receding horizon the values of LPSP 2 are significantly lower than LPSP 1. In fact, it is observed that the new strategy produce an improvement in the LPSP up to 88% for the case with $\rho = 50$.

6. Conclusions

This paper presents an energy management strategy to command the operation in a hybrid power system. The power system consists of two types of renewable sources (wind and solar) that operates as main power sources, and fuel cell modules and a battery bank as secondary power sources. The hydrogen for the fuel cells is produced from bioethanol reforming. The heat required for the reforming process is taken from the direct-current bus to improve the reforming efficiency.

The proposed strategy uses the concept of receding horizon and predictions of the future behavior of the renewable power sources and the load to improve the performance in terms of loss of power supply probability. The predictions are done using autoregressive models from historic data. In order to validate the performance of the strategy here proposed several simulation tests were performed and the results were compared with the results obtained in another strategy where predictions are not carried out. The results show a significantly improvement in the robustness of the power system. In fact, analyzing the capacity of satisfying the power balance, the new strategy presents an improvement in the power supply up to 88%, depending on the particular design.

Acknowledgment

The authors thank the financial support from CONICET, UNR-FCEIA, UTN-FRRo, and ANPCYT (PICT 2009-0017 and PICT 2012-0133).

References

[1] Borowy B, Salameh Z. Methodology for optimally sizing the combination of a battery bank and pv array in a wind/pv hybrid system. Energy conversion. IEEE Trans 1996;11(2):367–75.
[2] Boukhezzar B, Lupu L, Siguerdidjane H, Hand M. Multivariable control strategy for variable speed, variable pitch wind turbines. Renew Energy 2007;32(8):1273–87.
[3] Box G, Jenkins G, Reinsel G. Time series analysis: forecasting and control. 4th ed. John Wiley & Sons; 2008.
[4] Dursun E, Kilic O. Comparative evaluation of different power management strategies of a stand-alone PV/wind/PEMFC hybrid power system. Int J Electr Power & Energy Syst 2012;34(1):81–9.
[5] Ercot, 2013. Ercot – hourly load data archives. Available online. May 2013. accessed May 2013, http://www.ercot.com.
[6] Erdinc O, Elma O, Uzunoglu M, Selamogullari U, Vural B, Ugur E, et al. Experimental performance assessment of an online energy management strategy for varying renewable power production suppression. Int J Hydrog energy 2012;37(6):4737–48.
[7] Feroldi D, Degliuomini LN, Basualdo M. Energy management of a hybrid system based on wind-solar power sources and bioethanol. Chem Eng Res Des 2013;91(8):1440–55.
[8] Feroldi D, Zumoffen D. Sizing methodology for hybrid systems based on multiple renewable power sources integrated to the energy management strategy. Int J Hydrog Energy 2014;39:8609–20.
[9] Henson W. Optimal battery/ultracapacitor storage combination. J Power Sources 2008;179(1):417–23.
[10] Energy Homer. Energy modeling software for hybrid renewable energy systems. September 2012. Available online, accessed September 2012, http://www.homerenergy.com.
[11] Ipsakis D, Voutetakis S, Seferlis P, Stergiopoulos F, Elmasides C. Power management strategies for a stand-alone power system using renewable energy sources and hydrogen storage. Int J Hydrog Energy 2009;34(16):7081–95.
[12] Johnson V. Battery performance models in advisor. J Power Sources 2002;110(2):321–9.
[13] Khalid M, Savkin A. A model predictive control approach to the problem of wind power smoothing with controlled battery storage. Renew Energy 2010;35(7):1520–6.
[14] Koutroulis E, Kolokotsa D, Potirakis A, Kalaitzakis K. Methodology for optimal sizing of stand-alone photovoltaic/wind-generator systems using genetic algorithms. Sol energy 2006;80(9):1072–88.
[15] Larminie J, Dicks A. Fuel cell systems explained. 2nd ed. Wiley and Sons; 2003.
[16] Lei Y, Mullane A, Lightbody G, Yacamini R. Modeling of the wind turbine with a doubly fed induction generator for grid integration studies. IEEE Transaction Energy Convers 2006;21(1):257–63.
[17] Leyva R, Alonso C, Queinnec I, Cid-Pastor A, Lagrange D, Martinez-Salamero L. MPPT of photovoltaic systems using extremum-seeking control. Aerospace and electronic systems, IEEE. Trans 2006;42(1):249–58.
[18] Lujano-Rojas JM, Monteiro C, Dufo-López R, Bernal-Agustín JL. Optimum load management strategy for wind/diesel/battery hybrid power systems. Renew Energy 2012;44:288–95.
[19] Meteored. Global climate, climatic data worldwide. September 2012. Available online, accessed September 2012, http://clima.tiempo.com/.
[20] Nehrir MH, Wang C, Strunz K, Aki H, Ramakumar R, Bing J, et al. A review of hybrid renewable/alternative energy systems for electric power generation: configurations, control, and applications. IEEE Trans Sustain Energy 2011;2(4):392–403.
[21] Nelson D, Nehrir M, Wang C. Unit sizing and cost analysis of stand-alone hybrid wind/PV/fuel cell power generation systems. Renew Energy 2006;31(10):1641–56.
[22] Qi W, Liu J, Chen X, Christofides P. Supervisory predictive control of stand-alone wind/solar energy generation systems. Control systems technology. IEEE Trans 2011;19(1):199–207.
[23] Rullo P, Degliuomini LN, García M, Basualdo M. Model predictive control to ensure high quality hydrogen production for fuel cells. Int J Hydrog Energy 2014;39(16):8635–49.
[24] Schneider F. The state machine approach: a tutorial. 1990. Springer.
[25] Thounthong P, Chunkag V, Sethakul P, Sikkabut S, Pierfederici S, Davat B. Energy management of fuel cell/solar cell/supercapacitor hybrid power source. J Power Sources 2011;196(1):313–24.
[26] Torreglosa J, García P, Fernández L, Jurado F. Hierarchical energy management system for stand-alone hybrid system based on generation costs and cascade control. Energy Convers Manag 2014;77:514–26.
[27] Torreglosa JP, García P, Fernández LM, Jurado F. Energy dispatching based on predictive controller of an off-grid wind turbine/photovoltaic/hydrogen/battery hybrid system. Renew Energy 2015;74:326–36.
[28] Tsai H, Tu C, Su Y. Development of generalized photovoltaic model using MATLAB/SIMULINK. In: Proceedings of the world congress on engineering and computer science; 2008. p. 846–51.
[29] Valenciaga F, Puleston P. Supervisor control for a stand-alone hybrid generation system using wind and photovoltaic energy. Energy conversion. IEEE Trans 2005;20(2):398–405.
[30] Valenciaga F, Puleston P, Battaiotto P. Power control of a photovoltaic array in a hybrid electric generation system using sliding mode techniques. Control theory and applications. IEE Proceedings 2001;148(6):448–55.
[31] Valenciaga F, Puleston P, Battaiotto P, Mantz R. Passivity/sliding mode control of a stand-alone hybrid generation system. IEE Proc Control Theory Appl 2000;147(6):680–6.
[32] Wang X, Teichgraeber H, Palazoglu A, El-Farra NH. An economic receding horizon optimization approach for energy management in the chlor-alkali process with hybrid renewable energy generation. J Process Control 2014;24(8):1318–27.
[33] Yang H, Lu L, Burnett J. Weather data and probability analysis of hybrid photovoltaic–wind power generation systems in Hong Kong. Renew Energy 2003;28(11):1813–24.
[34] Zhou K, Ferreira J, De Haan S. Optimal energy management strategy and system sizing method for stand-alone photovoltaic-hydrogen systems. Int J Hydrog Energy 2008;33(2):477–89.